CONDENSED MATTER PHYSICS

Topological charge transport by mobile dielectric-ferroelectric domain walls

R. Takehara[1]*, K. Sunami[1], K. Miyagawa[1], T. Miyamoto[2], H. Okamoto[2,3], S. Horiuchi[4], R. Kato[5], K. Kanoda[1]*

The concept of topology has been widely applied in condensed matter physics, leading to the identification of peculiar electronic states on three-dimensional (3D) surfaces or 2D lines separating topologically distinctive regions. In the systems explored so far, the topological boundaries are built-in walls; thus, their motional degrees of freedom, which potentially bring about new paradigms, have been experimentally inaccessible. Here, working with a quasi-1D organic material with a charge-transfer instability, we show that mobile neutral-ionic (dielectric-ferroelectric) domain boundaries with topological charges carry strongly 1D-confined and anomalously large electrical conduction with an energy gap much smaller than the one-particle excitation gap. This consequence is further supported by nuclear magnetic resonance detection of spin solitons, which are required for steady current of topological charges. The present observation of topological charge transport may open a new channel for broad charge transport–related phenomena such as thermoelectric effects.

INTRODUCTION

The entanglement of charge, spin, and lattice degrees of freedom in condensed matter systems can bring about emergent excitations that are topological in character. The quasi–one-dimensional (1D) donor-acceptor mixed-stack complex tetrathiafulvalene-*p*-chloranil (TTF-CA) is a strongly coupled charge-spin-lattice system and exhibits a charge-transfer instability from the donor, TTF, to the acceptor, CA, by pressure (Fig. 1A) (*1*–*12*). In the neutral (N) phase stable at low pressures, the highest occupied molecular orbital (HOMO) of the TTF molecule is doubly occupied by electrons, whereas the lowest unoccupied molecular orbital (LUMO) of the CA molecule is empty, although charge is partially transferred from TTF to CA because of the hybridization of the orbitals. By contrast, in the ionic (I) phase that is stable at high pressures, each molecular orbital is singly occupied by a substantial electron transfer, which is caused by the Madelung energy gain. In the I phase, the spin degrees of freedom could be active but, in reality, are inactive by the spin-singlet formation due to the 1D lattice dimerization instabilities. Thus, the N phase at low pressures is a dielectric band insulator with inversion symmetry preserved, whereas the I phase appearing at high pressures is a dimerized spin-singlet Mott insulator with inversion symmetry broken, originating from strong Coulomb interactions and spin-lattice coupling (Fig. 1A) (*6*, *9*, *13*). The pressure-induced neutral-ionic (NI) transition is a first-order transition at low temperatures, but becomes a crossover at high temperatures (*7*, *11*, *12*). The I phase at high temperatures exhibits a dynamical donor-acceptor dimerization (*6*, *9*) and is distinguished from the low-temperature I phase with a static long-range dimerization order (*7*, *11*–*15*); the former (latter) is paraelectric (ferroelectric), denoted by the I_{para} (I_{ferro}) phase. The ferroelectricity mainly stemming from the charge transfer has been of current interest as electronic ferroelectricity (*16*–*18*).

This system is argued to have topological excitations such as kinks at the NI domain boundaries and solitons carrying charges and spins (*11*, *19*–*27*). It has been theoretically suggested that, at the NI transition, mobile NI (dielectric-ferroelectric) domain walls (NIDWs) with current-carrying topological charges originating from phase kinks in the charge density can be excited with much lower excitation energies than charge gaps in the two insulating phases (*19*). On the first-order NI transition at low temperatures and pressures, however, the 3D long-range dimerization order prohibits travel of the NIDWs. This is why electrical conduction by the NIDWs has long been experimentally elusive. If the N and I phases form dynamical domains by thermal excitations, however, then the mobile NIDWs can carry topological charge current. Thus, the NI crossover at high temperatures offers a region for testing the topological charge transport, as suggested by recent theoretical studies (*21*). A decrease in resistivity was reported in two-terminal measurements around this region (*23*, *25*). In the present study, we carry out four-terminal resistivity measurements of TTF-CA along three crystal axes under finely tuned pressure to reveal the topological charge transport of the NIDWs and perform ^{13}C-NMR (nuclear magnetic resonance) measurements to verify the involvement of spin solitons in the topological charge transport, as theoretically suggested (*21*, *22*, *28*).

RESULTS AND DISCUSSION

Enhancement and 1D confinement of electrical conduction at the NI crossover

First, we present a pressure-temperature phase diagram up to 35 kbar (Fig. 1A) constructed on the basis of the intrachain (*a*-axis) resistivity (Fig. 1B) and previous nuclear quadrupole resonance (NQR) studies (*7*, *11*, *12*). The temperature profile of the resistivity is different below and above approximately 9 kbar. Below 9 kbar, the resistivity is characterized by a kink between strongly insulating behavior at low temperatures and a moderate temperature dependence at high temperatures (section S1). The low-temperature behavior indicating a

[1]Department of Applied Physics, University of Tokyo, Bunkyo-ku, Tokyo 113-8656, Japan. [2]Department of Advanced Materials Science, University of Tokyo, Kashiwa, Chiba 277-8561, Japan. [3]AIST-UTokyo Advanced Operando–Measurement Technology Open Innovation Laboratory (OPERANDO-OIL), National Institute of Advanced Industrial Science and Technology (AIST), Chiba 277-8568, Japan. [4]Flexible Electronics Research Center (FLEC), National Institute of Advanced Industrial Science and Technology (AIST), Tsukuba, Ibaraki 305-8565, Japan. [5]Condensed Molecular Materials Laboratory, RIKEN, Wako, Saitama 351-0198, Japan.
*Corresponding author. Email: r.takehara@mdf2.t.u-tokyo.ac.jp (R.T.); kanoda@ap.t.u-tokyo.ac.jp (K.K.)

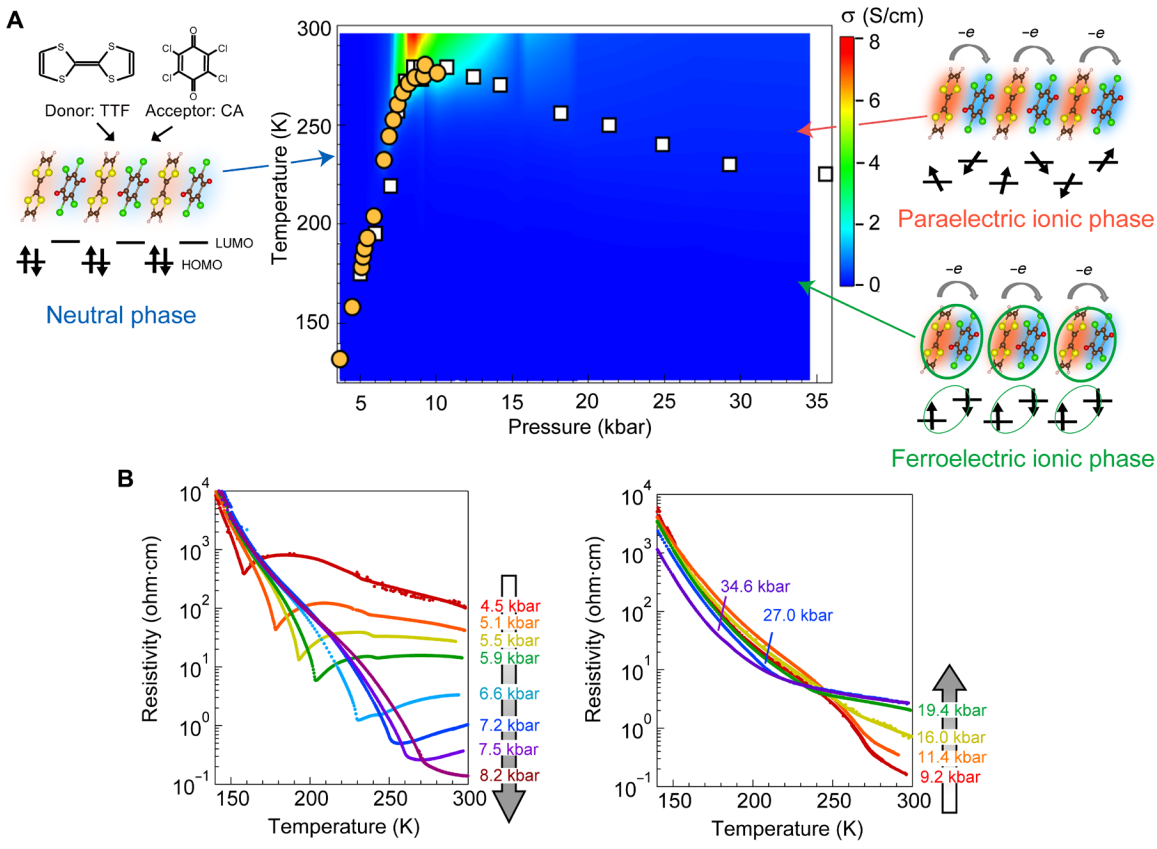

Fig. 1. Pressure-temperature phase diagram of TTF-CA and resistivity profiles. (**A**) Pressure-temperature (*P-T*) phase diagram consisting of three phases in TTF-CA. 1D alternating stacks of TTF and CA molecules show the N phase (left), I_{para} phase (top right), and I_{ferro} phase (bottom right). The colored clouds schematically drawn on the molecules show the hole density in the HOMO of the TTF molecule and the electron density in the LUMO of the CA molecule. In the *P-T* phase diagram (center), the orange circles indicate the positions of the kinks in the resistivity in (B), which correspond well to the dimerization transition points determined by previous nuclear quadrupole resonance (NQR) measurements (open squares) (*12*). The range of colors in the phase diagram indicates the magnitude of the conductivity. (**B**) Temperature dependence of the resistivity of TTF-CA along the *a* axis at pressures below (left) and above (right) 9 kbar.

large charge gap is robust against pressure, whereas the resistivity above the kink temperature is rapidly reduced down to the range of 0.1 to 1 ohm·cm, and the kink structure becomes less sharp with increasing pressure. As seen in Fig. 1A, the temperatures associated with the resistivity kinks (orange circles) correspond well to those of the long-range dimerization order detected by NQR (open squares) (*7*, *11*, *12*, *15*). For pressures above 9 kbar, the resistivity monotonously increases below room temperature without a clearly identifiable kink. The resistivity at high temperatures, above 250 K, increases with pressure, contrary to the behavior below 9 kbar. A contour plot of the absolute values of the conductivity (Fig. 1A) illustrates that a highly conducting state emerges in the crossover region. Figure 2 shows the pressure dependences of the *a* axis conductivity (Fig.2A) and the anisotropy of conductivity (Fig.2B) at room temperature. The geometries of electrodes against the crystal axis are depicted in Fig. 2C, D. We find that the *a* axis conductivity reaches a maximum value of 7 S/cm at 8.8 kbar (Fig. 2A), which is comparable to the room temperature conductivities of organic conductors. It is most remarkable that such a high conductivity appears between the two types of insulators.

The anisotropies of the conductivity, (σ_a/σ_b) and (σ_a/σ_c), shown in Fig. 2B, become highly 1D at approximately 9 kbar, where the *a*-axis conductivity is maximum (Fig. 2A), indicating that the charge transport is confined in the chains in the crossover region. The NIDW, which separates the neutral and ionic segments, carries a topological charge of $\rho_{NIDW} = \pm e(\rho_I - \rho_N)/2$ (*22*) and is mobile only within the 1D chain, where ρ_I and ρ_N are the molecular valences in the I and N phases, respectively, and *e* is the elementary charge. In general, the neutral and ionic segments are 3D-locked by long-range Coulomb interactions. As predicted theoretically, however, the interchain Coulomb coupling cancels out in TTF-CA because of the particular molecular arrangement in the *b-c* plane (*29*), allowing the NIDWs to travel freely. Optical measurements indicate that the neutral and ionic states dynamically coexist at approximately 9 kbar (*8*), consistent with mobile NIDWs.

Charge excitation gap

To further examine possible NIDW conduction, we measured the temperature dependence of the resistivity at 0.1-kbar intervals around the NI crossover pressure. Figure 3A shows the conductivity landscape, the magnitude of which is projected onto the *P-T* plane with a range of colors; the orange circles and gray line indicate the positions of the kinks and maxima in the *T* and *P* dependences of the conductivity, respectively. The kink positions coincide with the transition points of the long-range dimer order identified by the NQR measurements, whereas the gray line runs along the NI crossover line, where sharp charge transfer is detected by NQR and optical probes (*3*, *5*, *8*–*10*, *12*). We note that the infrared spectroscopy under

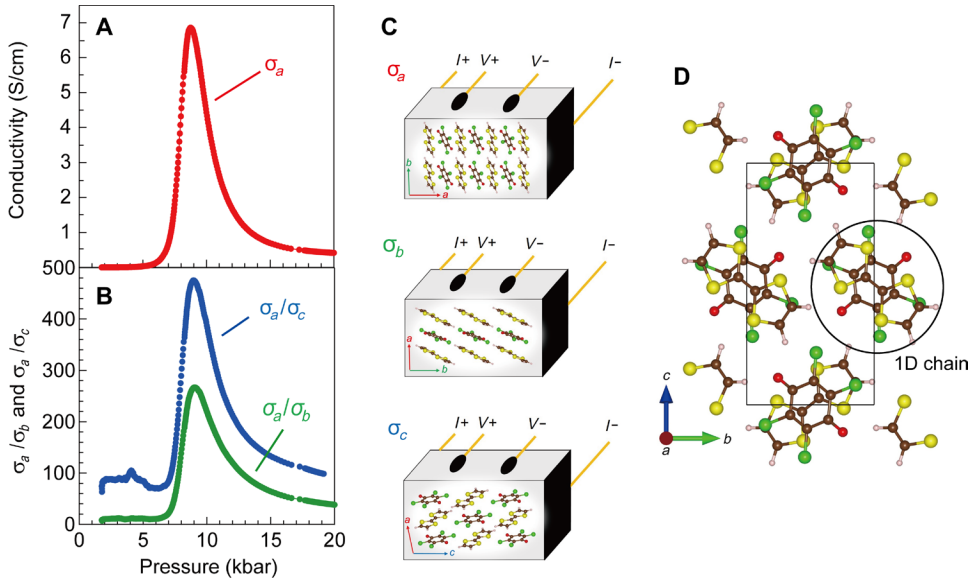

Fig. 2. Pressure dependence of the conductivity and its anisotropy in TTF-CA at room temperature. (**A**) Pressure dependence of the conductivity along the *a* axis. (**B**) Pressure dependence of the anisotropies of the conductivities defined as the ratio of conductivities along the *a* and *b* axes, σ_a/σ_b, and the ratio of conductivities along the *a* and *c* axes, σ_a/σ_c. (**C**) Schematics of electrical terminal configurations with respect to the molecular stacks in the resistivity measurements. Gold wires were attached on the side and top surfaces, using carbon paste, as current leads and voltage terminals, respectively. (**D**) Molecular arrangement of TTF and CA in the *b*-*c* plane perpendicular to the *a* axis (*13*).

pressure at room temperature (*6*, *9*) detected a steep increase in the molecular vibrational a_g mode, which is sensitive to the local dimer formation, at a pressure close to the gray line. Since the intensity of the a_g mode absorption measures the density of local dimers, that indicates a sharp increase in the dimer density at the pressure of the conductivity maxima; thus, the gray line denoted hereafter by $P_c(T)$ is regarded as the Widom line between a dimer gas and a dimer liquid as well as between the N phase and the I phase.

The NI crossover line (gray line) is tilted with respect to the *P* and *T* axes and interrupted by the appearance of the I_{ferro} phase, indicating that the long-range dimerization order suppresses anomalous conduction in the crossover (Fig. 3A). If the NIDW excitations are responsible for electrical conduction, then the conductivity should depend on the pressure deviation from the Widom line, P-P_c. Thus, we "corrected" the inclined boundary line $P_c(T)$ by taking $\Delta P = P(T) - P_c(T)$ as the pressure axis instead of *P*; the conductivity versus *P* at each *T* (Fig. 3B) is converted to conductivity versus ΔP (Fig. 3C). Figure 3D shows an Arrhenius plot of the conductivity along the NI boundary of $\Delta P = 0$ (the gray line in Fig. 3C), which yields an activation energy, E_g, of 0.055 eV. The values of E_g determined similarly for other pressures vary with ΔP, exhibiting a minimum at the NI boundary (Fig. 3E), reminiscent of the V-shaped profile of the charge-transfer (CT) excitations expected around the NI transition (*2*). However, the minimum value, 0.055 eV, is one order of magnitude smaller than the CT excitation energy, 0.6 to 0.7 eV (*2*, *30*), contradicting the one-particle charge excitations, thus invoking emergent excitations. Quantum Monte Carlo simulations predict NIDW excitation energies comparable to the present values with a V-shaped variation against the intersite Coulomb interaction (*19*), which is varied by pressure experimentally. The rounding of the V shape (Fig. 3E) is an effect of finite temperature; note that the simulation assumes a temperature of absolute zero. We note that band structure calculations for TTF-CA predict a bandgap of 0.52 eV (*2*, *30*–*32*), which is also much larger than the observed value.

Evaluation of the density of NIDWs

We estimate the density of thermally excited NIDWs by mapping the NI transition system to a 1D quantum XXZ antiferromagnetic spin model (*33*), which is further reduced to the Ising model, particularly for $V > 2t$, as in the present case, where *t* is the transfer integral between the donor and acceptor molecules (section S2). The NIDW corresponds to a spinon in the Ising spin system; thus, the correlation length in the Ising model, $\xi \sim 1/\ln(\coth(E_{DW}/2k_BT))$, measures the mean distance between the NIDWs; namely, the NIDW density is given by $n \sim 1/2\xi \sim \ln(\coth(E_{DW}/2k_BT))/2$. This form is approximately of the Arrhenius type for $E_{DW} > k_BT$ and rationalizes the activation-type temperature dependence of the conductivity, which is assumed to be proportional to the number of NIDWs. At room temperature, *n* yields one NIDW per approximately five donor-acceptor pairs, which explains the high conductivity in the NI crossover at room temperature. A more rigorous evaluation of *n* based on free energy consideration gives approximately the same value of *n* (section S2).

Mechanism of the topological charge transport

As was theoretically shown (*21*, *22*, *28*), stationary current necessitates spin solitons in ionic domains (Fig. 4, A and B, and section S3) (*26*). Solitonic spin excitations in TTF-CA were evidenced by NMR (*27*); the analyses of the NMR shift and relaxation rate, T_1^{-1}, found one spin soliton excited per 10 to 25 donor-acceptor pairs around the NI crossover. Since one NIDW per five donor-acceptor pairs means one ionic domain per 10 donor-acceptor pairs, it turns out that spin solitons and NIDWs are excited with comparable densities around P_c. To determine the spin soliton density in a wide pressure range across P_c, we measured ^{13}C-NMR T_1^{-1}, which probes local field fluctuations produced by electron spins, in more detail than previously performed (*27*). A single spectral species observed in the NMR spectrum represents motional narrowing due to the diffusive

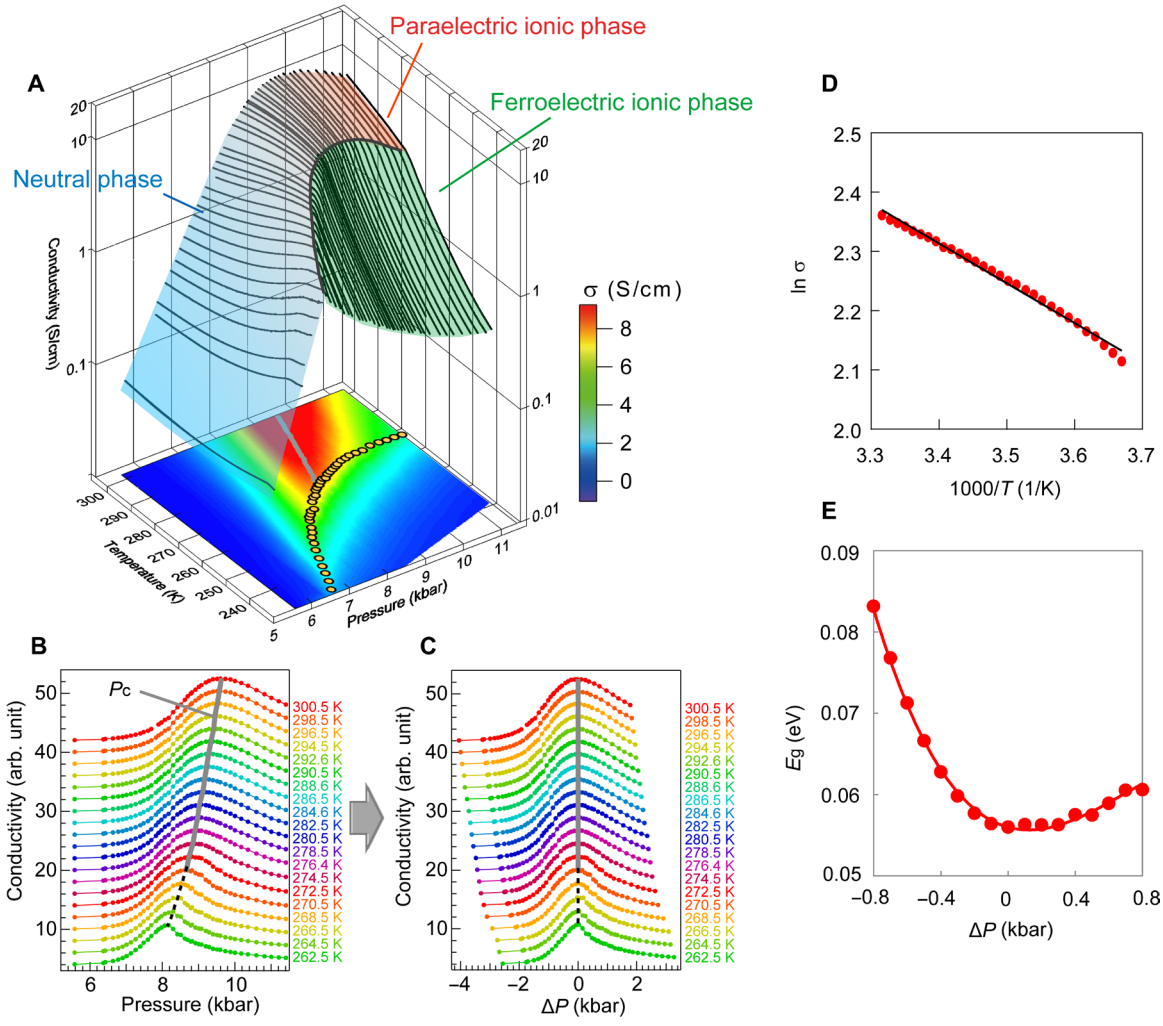

Fig. 3. Conductivity profile in the NI crossover region in TTF-CA. (**A**) Conductivity profile in the *P*-*T* plane. The black curves represent the temperature dependence of the conductivity for fixed pressures, which are set at approximately 0.1-kbar intervals in the range of 5.5 to 11.5 kbar. In the bottom panel, the range of colors indicates the magnitude of the conductivity; the gray line is the Widom line, $P_c(T)$, on which the conductivity is maximum with respect to pressure [also shown in (B)], and the orange circles indicate the dimerization transition points. (**B**) Traces of the conductivity as a function of pressure, *P*, at fixed temperatures. (**C**) Plot of the data in (B) as a function of $\Delta P = P - P_c$. Both in (B) and (C), the vertical axes are in arbitrary units, and the data plots for different temperatures are shifted vertically for clarity. (**D**) Arrhenius plot of the resistivity on the P_c line. The black line is a fit to the data, giving an estimate of the activation energy of 0.055 eV. (**E**) Activation energy as a function of ΔP.

motion of spin solitons (section S4). Considering that sparsely excited spin solitons should behave as free spins with negligible exchange interactions, the intensity of the local field fluctuations at a nuclear site, probed by T_1^{-1}, is proportional to the soliton density. As the pressure is increased, T_1^{-1} exhibits an exponential increase that parallels the conductivity for $P < P_c$ and then levels off in contrast to the decreasing conductivity for $P > P_c$ (Fig. 4B).

As the pressure decreases or increases from P_c, the minor phase domains (ionic for $P < P_c$ and neutral for $P > P_c$) become more sparsely excited, shrinking toward the solitons sandwiched by the NIDWs (Fig. 4B) (*34*), which are expected to govern charge transport at pressures away from P_c (*21*, *22*, *28*). For $P < P_c$, the excitations are NIDW-sandwiched spin solitons (or equivalently polarons) (Fig. 4B). Their dominant role in electrical conductivity is evidenced by the parallel increases in T_1^{-1} and conductivity for $P < P_c$ (Fig. 4B) [a donor-acceptor pair containing no spin soliton does not carry charges (section S3)]. For $P > P_c$, T_1^{-1} retains large values, which is indicative of a high spin soliton density. The decrease in conductivity that does not scale with the behavior of T_1^{-1} reflects a decrease in the excitations of the minor phase species, namely, charge solitons sandwiched by the NIDWs. Consistent with this expectation, the excitation energy of the charge solitons is theoretically indicated to increase as the system gets deeper into the ionic region far from the NI crossover (*21*) or transition (*22*). Thus, at pressures away from P_c, the conductivity is governed by spin solitons ($P < P_c$) or charge solitons ($P > P_c$). We note that, for $P > P_c$, resistivity shows no clear anomalies at the I_{para}-to-I_{ferro} transition upon cooling (Fig. 1B). This may be an indication that charge solitons survive in the form of polarons, which do not break the long-range dimer order, in the I_{ferro} phase.

Concluding remarks

A spin (charge) soliton can hop into a charge (spin) soliton site in an adjacent chain by transferring an electron, resulting in their exchange

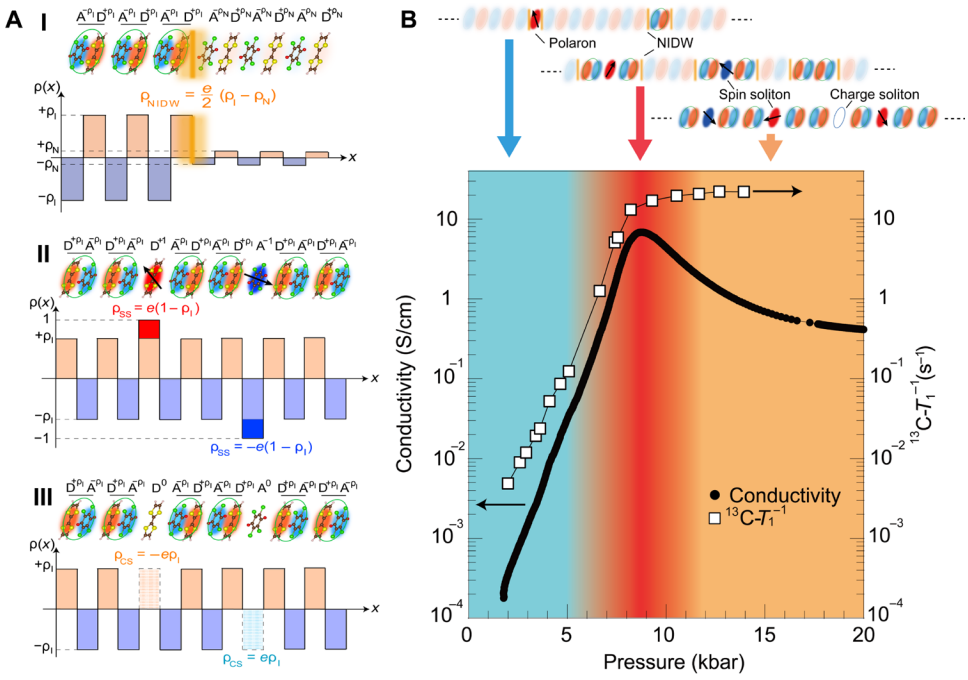

Fig. 4. Topological excitations carrying electrical currents and the pressure profile of the electrical conductivity and spin excitations. (**A**) Three types of topological excitations in the NI transition systems: NIDWs (I), spin solitons (II), and charge solitons (III). Donor and acceptor molecules are represented as D and A, respectively. The NIDW has an effective charge of $\pm e(\rho_I - \rho_N)/2$, where ρ_I and ρ_N are the degrees of charge transfer in the ionic and neutral states, respectively, and are 0.7 to 0.8 and 0.3 to 0.4 around the NI crossover (*8*, *9*). The spin and charge solitons have effective charges of $\pm e(1 - \rho_I)$ and $\pm e\rho_I$, respectively, corresponding to excessive and deficient charges from the dimerized-ionic background, as depicted. These charges are called topological charges, as their fractional nature has the topological origin in the charge degrees of freedom; however, they take noninvariant values and thus are distinguished from the topological charge characterized by quantum numbers. (**B**) Pressure dependence of the conductivity (black circles) and ^{13}C-NMR T_1^{-1} (open squares) at room temperature. The mechanism of electrical conduction is divided into three regimes: In the N phase at low pressures (blue-colored region), spin solitons sandwiched by NIDWs (called polarons), which carry both charges and spins, are sparsely excited in the neutral background and lead to electrical conduction. In the NI crossover region at middle pressures (red-colored region), the NIDWs and spin solitons are excited with comparable densities and carry electrical currents (section S3). In the I phase at high pressures (orange-colored region), the charge solitons are sparsely excited in the ionic background and, in conjunction with more densely excited spin solitons, carry electrical currents.

(e.g., between II and III in Fig. 4A), which is expected to give conventional electron current in the transverse direction. In contrast, unbound NIDWs resulting from the fractionalization of solitons around P_c have no way to hop into adjacent chains, resulting in highly 1D transport confined in the chain around P_c, as observed here. The charge transport by the topological excitations distinct from the conventional quasiparticles is possible particularly in 1D where the topological boundaries are in the form of points, which are mobile. The exotic nature and pressure controllability of such transport are expected to open a new door to a wide range of charge transport–related issues; for example, the thermoelectric effect by topological charge excitations may give a new channel in developing thermoelectric materials with high performance. A large thermoelectric effect by a topological spin texture is reported (*35*).

MATERIALS AND METHODS

Sample preparation

Single crystals of TTF-CA were prepared by a cosublimation method for both ^{13}C-enriched and non-enriched samples; ampules containing the purified compounds were set in a vacuum-sealed glass tube, which were heated with a three-zone temperature-controlled furnace. In the ^{13}C-enriched sample, the central double-bonded carbon atoms in TTF were substituted by ^{13}C isotopes with a 99% concentration (*27*).

Electrical resistivity measurements under pressure

Resistivity measurements of TTF-CA were performed for single crystals with the four-terminal method. Hydrostatic pressure was applied to the sample using a BeCu/NiCrAl dual-structured clamp-type cell with Daphne 7373 ($P < 20$ kbar) and Daphne 7474 (20 kbar $< P <$ 35 kbar) oils as the pressure media. The solidification pressures of the Daphne 7373 and Daphne 7474 oils are approximately 22 and 37 kbar at room temperature, respectively (*36*). In the measurements in the wide range of pressures displayed in Figs. 1 and 2, we monitored the external pressure during the pressurization at room temperature and converted it to internal pressure using a pressure efficiency of 0.9, which was separately determined by the resistance of a Manganin wire mounted in the pressure cell. In the measurements under the finely tuned pressures displayed in Fig. 3, we monitored the inner pressure through the resistance of a Manganin wire mounted with the sample in the same cell. The pressure values indicated in the main text are the internal pressures determined at room temperature.

^{13}C-NMR measurements under pressure

We conducted ^{13}C-NMR measurements for a TTF-CA single crystal, in which the central double-bonded carbon sites in TTF molecules were enriched by ^{13}C isotopes. A magnetic field of 8 T was applied in a direction approximately 35° tilted from the *a* axis to the *c* axis. We used the so-called solid-echo pulse sequence of $(\pi/2)_x$-τ-$(\pi/2)_y$

to acquire the ^{13}C-NMR signals, where $(\pi/2)_i$ means a $\pi/2$ pulse of a radio frequency wave applied along the i axis in the rotational frame and τ is the time interval between the two $\pi/2$ pulses. The nuclear spin-lattice relaxation rate T_1^{-1} was measured by the standard saturation recovery method. The relaxation curve of nuclear magnetization was well fitted by a single exponential function for every pressure studied (section S4). We used a clamp-type pressure cell made of nonmagnetic BeCu to apply hydrostatic pressure to the sample. The pressure medium used was Daphne 7373 oil. The pressure values quoted in the main text are the room temperature values.

SUPPLEMENTARY MATERIALS

Supplementary material for this article is available at http://advances.sciencemag.org/cgi/content/full/5/11/eaax8720/DC1

Section S1. Temperature dependence of the resistivity
Section S2. Analysis of the conductivity in the NI transition region in terms of the Ising model
Section S3. Electrical current by the NIDW and spin soliton excitations
Section S4. ^{13}C-NMR spectra and relaxation curves of nuclear magnetization
Fig. S1. Temperature dependence of the resistivity in the NI crossover region.
Fig. S2. Correspondence between molecular states and virtual spins.
Fig. S3. Fitting of the temperature dependence of the conductivity by the 1D ferromagnetic spin model.
Fig. S4. Schematic of the transport of NIDWs and spin solitons that contribute to the electrical conductivity.
Fig. S5. Schematic of the transport of NIDWs that do not contribute to the electrical conductivity.
Fig. S6. ^{13}C-enriched TTF molecule, ^{13}C-NMR spectrum, and relaxation curve.

REFERENCES AND NOTES

1. H. M. McConnell, B. M. Hoffman, R. M. Metzger, Charge transfer in molecular crystals. *Proc. Natl. Acad. Sci. U.S.A.* **53**, 46–50 (1965).
2. J. B. Torrance, J. E. Vazquez, J. J. Mayerle, V. Y. Lee, Discovery of a neutral-to-ionic phase transition in organic materials. *Phys. Rev. Lett.* **46**, 253–257 (1981).
3. Y. Tokura, H. Okamoto, T. Koda, T. Mitani, Pressure-induced neutral-to-ionic phase transition in TTF-*p*-chloranil studied by infrared vibrational spectrocopy. *Solid State Commun.* **57**, 607–610 (1986).
4. A. Girlando, C. Pecile, A. Brillante, K. Syassen, Neutral-ionic interface in mixed stack charge transfer compounds: Pressure induced ionic phase of tetrathiafulvalene-chloranil (TTF-CA). *Solid State Commun.* **57**, 891–896 (1986).
5. Y. Kaneko, S. Tanuma, Y. Tokura, T. Koda, T. Mitani, G. Saito, Optical reflectivity spectra of the mixed-stack organic charge-transfer crystal tetrathiafulvalene-*p*-chloranil under hydrostatic pressure. *Phys. Rev. B* **35**, 8024–8029 (1987).
6. H. Okamoto, T. Koda, Y. Tokura, T. Mitani, G. Saito, Pressure-induced neutral-to-ionic phase transition in organic charge-transfer crystals of tetrathiafulvalene-*p*-benzoquinone derivatives. *Phys. Rev. B* **39**, 10693–10701 (1989).
7. M. H. Lemée-Cailleau, M. Le Cointe, H. Cailleau, T. Luty, F. Moussa, J. Roos, D. Brinkmann, B. Toudic, C. Ayache, N. Karl, Thermodynamics of the neutral-to-ionic transition as condensation and crystallization of charge-transfer excitations. *Phys. Rev. Lett.* **79**, 1690–1693 (1997).
8. H. Matsuzaki, H. Takamatsu, H. Kishida, H. Okamoto, Valence fluctuation and domain-wall dynamics in pressure-induced neutral-to-ionic phase transition of organic charge-transfer crystal. *J. Phys. Soc. Jpn.* **74**, 2925–2928 (2005).
9. M. Masino, A. Girlando, A. Brillante, Intermediate regime in pressure-induced neutral-ionic transition in tetrathiafulvalene-chloranil. *Phys. Rev. B* **76**, 064114 (2007).
10. A. Dengl, R. Beyer, T. Peterseim, T. Ivek, G. Untereiner, M. Dressel, Evolution of ferroelectricity in tetrathiafulvalene-*p*-chloranil as a function of pressure and temperature. *J. Chem. Phys.* **140**, 244511 (2014).
11. M. Buron-Le Cointe, E. Collet, B. Toudic, P. Czarnecki, H. Cailleau, Back to the structural and dynamical properties of neutral-ionic phase transitions. *Crystals* **7**, 285 (2017).
12. R. Takehara, K. Sunami, F. Iwase, M. Hosoda, K. Miyagawa, T. Miyamoto, H. Okamoto, K. Kanoda, Revisited phase diagram on charge instabilit and lattice symmetry breaking in the organic ferroelectric TTF-QCl_4. *Phys. Rev. B* **98**, 054103 (2018).
13. M. Le Cointe, M. H. Lemée-Cailleau, H. Cailleau, B. Toudic, L. Toupet, G. Heger, F. Moussa, P. Schweiss, K. H. Kraft, N. Karl, Symmetry breaking and structural changes at the neutral-to-ionic transition in tetrathiafulvalene-*p*-chloranil. *Phys. Rev. B* **51**, 3374–3386 (1995).
14. J. Gallier, B. Toudic, Y. Délugeard, H. Cailleau, M. Gourdji, A. Péneau, L. Guibé, Chlorine-nuclear-quadrupole-resonance study of the neutral-to-ionic transition in tetrathiafulvalene-chloranil. *Phys. Rev. B* **47**, 11688–11695 (1993).
15. T. Luty, H. Cailleau, S. Koshihara, E. Collet, M. Takesada, M. H. Lemée-Cailleau, M. Buron-Le Cointe, N. Nagaosa, Y. Tokura, E. Zienkiewicz, B. Ouladdiaf, Static and dynamic order of cooperative multi-electron transfer. *Europhys. Lett.* **59**, 619–625 (2002).
16. K. Kobayashi, S. Horiuchi, R. Kumai, F. Kagawa, Y. Murakami, Y. Tokura, Electronic ferroelectricity in a molecular crystal with large polarization directing antiparallel to ionic displacement. *Phys. Rev. Lett.* **108**, 237601 (2012).
17. S. Ishibashi, K. Terakura, First-principles study of spontaneous polarization in tetrathiafulvalene-*p*-chloranil (TTF-CA). *Physica B Condens. Matter* **405**, S338–S340 (2010).
18. K. Terakura, S. Ishibashi, Mechanism of covalency-induced electric polarization within the framework of maximally localized Wannier orbitals. *Phys. Rev. B* **91**, 195120 (2015).
19. N. Nagaosa, J.-i. Takimoto, Theory of neutal-ionic transition in organic crystals. II. Effect of the intersite coulomb interaction. *J. Phys. Soc. Jpn.* **55**, 2745–2753 (1986).
20. Z. G. Soos, A. Painelli, Metastable domains and potential energy surfaces in organic charge-transfer salts with neutral-ionic phase transitions. *Phys. Rev. B* **75**, 155119 (2007).
21. H. Fukuyama, M. Ogata, Solitons in the crossover between band insulator and Mott insulator: Application to TTF-chloranil under pressure. *J. Phys. Soc. Jpn.* **85**, 023702 (2016).
22. M. Tsuchiizu, H. Yoshioka, H. Seo, Phase competition, solitons, and domain walls in neutral-ionic transition systems. *J. Phys. Soc. Jpn.* **85**, 104705 (2016).
23. T. Mitani, Y. Kaneko, S. Tanuma, Y. Tokura, T. Koda, G. Saito, Electric conductivity and phase diagram of a mixed stack charge transfer crystal: Tetrathiafulvalene-*p*-cholranil. *Phys. Rev. B* **35**, 427(R)–429(R) (1987).
24. Y. Tokura, H. Okamoto, T. Koda, T. Mitani, G. Saito, Nonlinear electric transport and switching phenomenon in the mixed stack charge transfer crystal tetrathiafulvalene-*p*-chloranil. *Phys. Rev. B* **38**, 2215(R) (1988).
25. H. Okamoto, T. Komatsu, Y. Iwasa, T. Koda, Y. Tokura, S. Koshihara, T. Mitani, G. Saito, Dynamical aspects of neutral-ionic phase transition in organic charge-transfer complex crystals. *Synth. Met.* **27**, 189–196 (1988).
26. H. Okamoto, T. Mitani, Y. Tokura, S. Koshihara, T. Komatsu, Y. Iwasa, T. Koda, G. Saito, Anomalous dielectric response in tetrathiafulvalene-*p*-chloranil as observed in temperature and pressure induced neutral to ionic phase transition. *Phys. Rev. B* **43**, 8224–8232 (1991).
27. K. Sunami, T. Nishikawa, K. Miyagawa, S. Horiuchi, R. Kato, T. Miyamoto, H. Okamoto, K. Kanoda, Evidence for solitonic spin excitations from a charge-lattice-coupled ferroelectric order. *Sci. Adv.* **4**, eaau7725 (2018).
28. N. Nagaosa, Theory of neutral-ionic transition in organic crystals. III. Effect of the electron-lattice interaction. *J. Phys. Soc. Jpn.* **55**, 2754–2764 (1986).
29. N. Nagaosa, Theory of neutral ionic transition in organic crystals. IV. Phenomenological viewpoint. *J. Phys. Soc. Jpn.* **55**, 3488–3497 (1986).
30. H. Okamoto, Y. Ishige, S. Tanaka, H. Kishida, S. Iwai, Y. Tokura, Photoinduced phase transition in tetrathiafulvalene-*p*-chloranil observed in femtosecond reflection spectroscopy. *Phys. Rev. B* **70**, 165202 (2004).
31. C. Katan, C. Koenig, P. E. Blöchl, Ab-initio calculations of one-dimensional band structures of mixed-stack molecular crystal. *Solid State Commun.* **102**, 589–594 (1997).
32. V. Oison, C. Katan, P. Rabiller, M. Souhassou, C. Koenig, Neutral-ionic phase transition: A thorough ab initio study of TTF-CA. *Phys. Rev. B* **67**, 035120 (2003).
33. R. Bruinsma, P. Bak, J. B. Torrance, Neutral-ionic transitions in organic mixed-stack compounds. *Phys. Rev. B* **27**, 456–466 (1983).
34. M. Buron-Le Cointe, M. H. Lemée-Cailleau, H. Cailleau, S. Ravy, J. F. Bérar, S. Rouzière, E. Elkaïm, E. Collet, One-dimensional fluctuating nanodomains in the charge-transfer molecular system TTF-CA and their first-order crystallization. *Phys. Rev. Lett.* **96**, 205503 (2006).
35. Y. Fujishiro, N. Kanazawa, T. Shimojima, A. Nakamura, K. Ishizaka, T. Koretsune, R. Arita, A. Miyake, H. Mitamura, K. Akiba, M. Tokunaga, J. Shiogai, S. Kimura, S. Awaji, A. Tsukazaki, A. Kikkawa, Y. Taguchi, Y. Tokura, Large magneto-thermopower in MnGe with topological spin texture. *Nat. Commun.* **9**, 408 (2018).
36. K. Murata, K. Yokogawa, H. Yoshino, S. Klotz, P. Munsch, A. Irizawa, M. Nishiyama, K. Iizuka, T. Nanba, T. Okada, Y. Shiraga, S. Aoyama, Pressure transmitting medium Daphne 7474 solidifying at 3.7 GPa at room temperature. *Rev. Sci. Instrum.* **79**, 085101 (2008).

Acknowledgments: We thank N. Nagaosa, A. Maeda, F. Kagawa, M. Hosoda, T. Nishikawa, and H. Fukuyama for fruitful discussions. **Funding:** This work was supported by the JSPS Grants-in-Aid for Scientific Research (S) (grant nos. JP25220709, JP16H06346, and JP18H05225) and for Scientific Research (C) (grant no. JP17K05532); by CREST (grant no. JPMJCR1661), Japan Science and Technology Agency; and by the Murata Science Foundation. **Author contributions:** R.T. performed the electrical resistivity

measurements, and K.S. and K.M. carried out the NMR measurements. R.K. synthesized the ^{13}C-enriched TTF molecules. T.M., H.O., and S.H. prepared the TTF-CA single crystals. R.T. wrote the manuscript with the assistance of K.S., K.M., and K.K. R.T., K.M., and K.K. designed the experiments. All authors discussed the results and commented on the manuscript. This project was headed by K.K. **Competing interests:** The authors declare that they have no competing interests. **Data and materials availability:** All data needed to evaluate the conclusions in the paper are present in the paper and/or the Supplementary Materials. Additional data related to this paper may be requested from the authors.

Submitted 30 April 2019
Accepted 19 September 2019
Published 15 November 2019
10.1126/sciadv.aax8720

Citation: R. Takehara, K. Sunami, K. Miyagawa, T. Miyamoto, H. Okamoto, S. Horiuchi, R. Kato, K. Kanoda, Topological charge transport by mobile dielectric-ferroelectric domain walls. *Sci. Adv.* **5**, eaax8720 (2019).